CALPHAD: Computer Coupling of Phase Diagrams and Thermochemistry 35 (2011) 72–81

Contents lists available at ScienceDirect

CALPHAD: Computer Coupling of Phase Diagrams and Thermochemistry

journal homepage: www.elsevier.com/locate/calphad

The thermodynamics of several elements at high pressure

A. Karbasi *, S.K. Saxena, R. Hrubiak

Center for the Study of Matter at Extreme Conditions, Florida International University, Miami, FL 31999, United States

ARTICLE INFO

Article history:
Received 22 August 2010
Received in revised form
27 November 2010
Accepted 27 November 2010
Available online 21 December 2010

Keywords:
High pressure
Explicit Gibbs free energy
Equation of state

ABSTRACT

We have used the CALPHAD-compatible equation of state (EOS) based on the explicit Gibbs free energy concept for the solid state of ten important elements: V, Nb, Ta, Mo, W (groups VB and VIB), Pd, Pt (group VIIIB) and Cu, Ag and Au (group IB). The new formulation uses SGTE data for ambient pressure and converges to the quasi-harmonic model at the limit of extreme pressure to calculate the Gibbs free energy as a function of pressure and temperature. The model is based on the available pressure–volume–temperature (*PVT*) data on the elements and can be usefully extrapolated to extreme pressures. When compared to shock wave data, the modeled EOS holds well, but the fit is not totally satisfactory in the ultrahigh-pressure range. A great advantage of this formulation is that it can be used to calculate thermodynamic properties such as the heat capacity and entropy at very high temperatures and pressures.

1. Introduction

The current CALPHAD [1] technique is based on the Gibbs free energy, with temperature and pressure as its variables. The Gibbs free energy in high-pressure and high-temperature conditions can be calculated in CALPHAD methodology by the so-called "explicit Gibbs free energy equation of state (EOS)" [2], and is written as

$$G(P,T) = G(P_0,T) + \int_{P_0}^{P} V(P',T)\mathrm{d}P', \quad (1)$$

where $G(P_0,T)$ is the Gibbs free energy along the reference isobar (usually 1 atm), and it can be calculated from different thermodynamic databases. The volumetric integral's calculation needs a relationship among different thermodynamic variables. Various EOSs [2–13] have been used to overcome this problem, but manifestly wrong predictions of thermophysical properties at high pressure, like negative heat capacity and thermal expansion [12] as shown in Fig. 1 for the heat capacity of tungsten at high pressure ($P = 500$ GPa), indicate their failure. On the other hand, instead of using Eq. (1) to solve the volumetric integral, the total Helmholtz free energy can be used. Lu and co-workers [12–16] used the Debye–Grüneisen model and successfully predicted the thermophysical properties of Cu without any anomaly at high pressure. In this way, new databases are needed to calculate thermodynamic and thermophysical properties.

It would be ideal and more convenient to formulate the Gibbs free energy directly as a function of temperature and pressure instead of using separate volumetric databases. In thermodynamic databases like the SGTE database [19], the reappearance of solid phases above the melting temperature is avoided by decreasing the solid heat capacity and then ultimately converging it to a fixed value. But the heat capacity above the melting point is beyond the experimental measurable range; extrapolation is uncontrollable and can never be compared with experimental results [11]. Since there is no standard theoretical approach to construct such an approximation, it is inherently problematic, and the results are inconsistent. It was shown [10] that this extrapolation of SGTE databases is incompatible with the famous Mie–Grüneisen equation [8], which is mostly used as an extension to high-pressure conditions, and leads to unphysical predictions of negative isobaric heat capacity.

Brosh et al. [10,11,20,21] developed a new formulation that uses SGTE data for ambient pressure and converges to the quasi-harmonic model at the limit of extreme pressure, and proposed a new formulation for incorporation of high pressure in CALPHAD terminology. We describe their model briefly in the following section, and use it to study the high-pressure behavior of the solid-state behavior of ten elements from groups IB, VB, VIB and VIIIB of the periodic table. It should be noted that Cr and Ni are excluded from this study due to the scarcity of experimental data on the thermal dependence of the bulk modulus, but if there were such data it would be interesting to examine the behavior of magnetic elements at high pressure with the proposed model.

2. Equation of state

In the proposed EOS, volume should be written as the sum of the cold compression volume and the thermal volume [10]:

$$V(P,T) = V_c(P,T_0) + V_{th}(P,T), \quad (2)$$

* Corresponding author. Tel.: +1 646 709 3983; fax: +1 305 348 3070.
E-mail address: ali.karbasi@fiu.edu (A. Karbasi).

0364-5916/$ – see front matter © 2010 Elsevier Ltd. All rights reserved.
doi:10.1016/j.calphad.2010.11.007

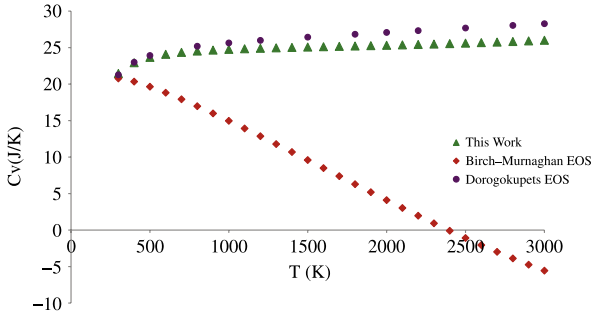

Fig. 1. Heat capacity of tungsten at 500 GPa and at high temperature using different EOSs. (♦) Birch–Murnaghan EOS with the data from [7,17], (●) Dorogokupets et al. EOS [18], (▲) EOS proposed in this work.

where $V_c(P, T_0)$ is the cold compression volume as shown in Eq. (3), and is determined by molar volume (V_0), the bulk modulus (B_0), and its first pressure derivative (B_0'), taken at zero pressure and at the reference temperature T_0 (300 K). The cold compression curve also should converge to the Thomas–Fermi-type models at very high pressure.

$$V(0,P) = V_0 \cdot \sum_{n=2}^{5} c_n [X_n(B_0, B_0', P)]^3 = V_0 \cdot \sum_{n=2}^{5} c_n \left[1 - a_n + a_n \cdot \left(1 + \frac{n}{3a_n} \cdot \frac{P}{B_0}\right)^{\frac{1}{n}}\right]^{-3}, \quad (3)$$

where $a_n = (n-1)\cdot(3B_0' - 1)^{-1}$ and c_n (i.e., c_2, c_3, c_4 and c_5) is calculated parameter depend on Z, V_0, B_0 and B_0', and is completely described in [10]. The other term is the thermal volume ($V_{th}(P, T)$). The isobaric heat capacity, thermal expansion coefficient and compressibility should all be positive, except in some unusual cases. Therefore, the thermal volume should be chosen to fulfill this condition. In addition to that, it should also satisfy an increasing compressibility with increasing temperature and decreasing thermal expansion and heat capacity with rising pressure. The heat capacity also should reach a finite value at infinite pressure [11].

The first step in evaluating the Gibbs free energy at the desired state of pressure and temperature is to calculate the addition of Gibbs free energy associated by integration of cold compression from the reference pressure to the extreme pressure. The next step is the isobaric integration of the heat capacity up to the desired temperature. Finally, by integrating backwards over pressure at the desired temperature, one attains the target thermodynamic state. The Gibbs free energy over this entire pass can be written as

$$G(T,P) = G_C(P) + G^{QH}(T,P) - [G^{QH}(T,P_0) - G(T,P_0)]\cdot I(P), \quad (4)$$

where the first term is the increase of Gibbs free energy due to cold compression from P_0 to P, which can be calculated from the integration of Eq. (3), G^{QH} is the increase of Gibbs free energy due to integration of the heat capacity at very high pressure, and the last term accounts for the backward integration of thermal volume; $I(P)$ is a interpolation function.

At ultrahigh pressure, the isobaric heat capacity converges to the isochoric heat capacity, and the Gibbs free energy can be written analogously to the famous quasi-harmonic Helmholtz free energy [8] as

$$G^{QH}(T,P) = 3NRT \cdot \ln\left[1 - \exp\left(-\frac{\theta(P)}{T}\right)\right], \quad (5)$$

where N is the number of atoms per unit of molecular formula, θ is the pressure-dependent Einstein temperature, which can be written as

$$\theta = \theta_0 \cdot \exp\left\{\frac{\gamma_0}{1+\delta_0}[\Gamma_2(b_0, X_2^T) - \Gamma_2(b_0, 1)]\right\}, \quad (6)$$

while $\Gamma_2(b_0, X_2^T) - \Gamma_2(b_0, 1) = \frac{1+\delta_0}{B_0}\int_0^p (X_2^T)^3 dP'$ and $X_2^T = [1 - \frac{1}{3b_0-1} + \frac{1}{3b_0-1}\cdot(1 + \frac{2}{3}\frac{3b_0-1}{1+\delta_0}\frac{P}{B_0})^{\frac{1}{2}}]^{-1}$ is same as X_n which is used in Eq. (3) with $n = 2$; θ_0, γ_0, δ_0, and b_0 are model parameters. One can say that θ_0, γ_0, and δ_0 are related to the Einstein characteristic temperature, Grüneisen parameter, and Anderson–Grüneisen parameter, respectively [10]. At quite high temperature ($T \gg 2\theta$) V^{QH} can be simplified as

$$V^{QH}(T > 2\theta, 0) = 3NRT\frac{d\ln(\theta)}{dP} = TV_0\alpha_0(X_2^T)^3, \quad (7)$$

where $\alpha_0 = 3NR\gamma_0/B_0V_0$ is thermal expansion coefficient at ambient pressure and moderate temperature above θ_0.

The total value of the thermal volume is sum of V^{QH} and the interpolation volume due to the change of Gibbs free energy expressed in the square-bracketed term of Eq. (4). The last term in Eq. (4) arises from the difference between the actual heat capacity at normal pressure $C_P(T, P_0)$ and the quasi-harmonic heat capacity due to G^{QH} at the same conditions, and it can expressed as

$$V^{\text{Interp}}(T,P) = -C(T)\cdot\frac{dI(P)}{dP}, \quad (8)$$

where $C(T) = G^{QH}(T,P_0) - G(T,P_0) = \int_0^T\int_0^{T'}\frac{1}{T''}[C_P(T,P_0) - C_P^{QH}(T,P_0)]dT''dT'$ and $I(P)$ is a monotonically decreasing and dimensionless interpolation function with the limiting values $I(0) = 1, I(\infty) = 0$, expressed as

$$I(P) = \frac{1}{1+b_1}\cdot\left\{b_1 + \left[1 + 2\cdot b_1\cdot(1+\delta_1)\frac{P}{B_0}\right]^{\frac{1}{2}}\right\} \cdot \exp\left\{\frac{1}{b_1} - \frac{1}{b_1}\left[1 + 2\cdot b_1\cdot(1+\delta_1)\frac{P}{B_0}\right]^{\frac{1}{2}}\right\}, \quad (9)$$

where δ_1 and b_1 are additional adjustable parameters of the EOS. Brosh et al. [10,21] suggested calculating these parameters from the high-temperature thermal expansion and bulk modulus at normal pressure, using Eqs. (10) and (11). At ambient pressure, the thermal expansion can be written as

$$\alpha = \frac{1}{V}\frac{dV(T \gg 2\theta, 0)}{dT} = \alpha_0 + \frac{dC(T)}{dT}\cdot\frac{1+\delta_1}{B_0V_0(1+b_1)} = \alpha_0 + \alpha_1 \quad (10)$$

and the bulk modulus can be calculated by series expansion, and is expressed as

$$B(T \gg 2\theta, 0) = B_0 - B_0\alpha_0\delta_0T - B_0\alpha_1\delta_1T. \quad (11)$$

We found that δ_1 calculated from Eq. (11) tends to have negative value in many cases, especially in high-temperature data; therefore we suggest replacing Eq. (11) with the following equation:

$$\delta_1 = -\frac{1}{\alpha_1}\left[\frac{1}{B_0}\frac{dB}{dT} + \delta_0\alpha_0\right]. \quad (12)$$

δ_1 resembles δ_0 at quite high temperature. The parameters b_0 and b_1 in the EOS control the thermal expansion at high pressure. Although b_0 and b_1 have no direct counterpart in conventional EOS models, their values are probably related to the volume dependence of the Grüneisen parameter. Therefore the initial value of 1 for both of them will be a good starting point for adjusting them [10].

It should be noted that the proposed functions in Eq. (4) imply a monotonic decrease of the heat capacity from its value at the reference condition to its final limit at infinite pressure. In addition to that, negative heat capacity is avoided due to the

Table 1
EOS parameters for the ten elements.

Element	*Z*	V_0	B_0	B'	c_2	c_3	c_4	c_5	θ_0	γ_0	δ_0	b_0	δ_1	b_1
Mo	42	9.345	243	4.57	−0.001	0.549	−0.638	1.090	273.7	1.7055	4.0947	1	3.5908	1.25163
W	74	9.525	296	4.4	0.275	−0.575	0.250	1.049	232	1.64	4.15	1	5.1	0.055345
V	23	8.31	162	3.5	0.3532	−0.90108	0.52390	1.02391	271.7	1.385	4.100	1	6.7	1
Nb	41	10.77	168.8	3.3	0.35478	−0.69126	−0.11925	1.45573	300	1.536	3.610	1	2.5	0.5
Ta	73	10.79	192	3.69	0.45911	−1.11478	0.2123	1.44333	160.9	1.558	8.798	1	1.823	0.015
Pd	46	8.8	183	5.28	0.021	0.328	−0.177	0.827	201.5	2.3991	2.3965	1	1.5	1
Pt	78	9.04	279	5.03	0.136	−0.109	0.096	0.875	179	2.6665	10.8865	1	6.434	1
Cu	29	7.05	133	5.37	0.1563	−0.3714	0.7074	0.5077	230.2	1.7784	5.9705	1	12.4065	1.5
Ag	47	10.1	99.32	5.89	−0.028	0.499	−0.240	0.769	163.6	2.6356	6.077	1	8.4533	3.052406
Au	79	10.12	167	5.31	2.58E−05	0.447	−0.343	0.896	129.3	2.3959	8.5583	1	10.0434	0.702442

inherently larger value of the actual heat capacity in comparison with $C_P^{QH}(T, P_0)$.

3. Determination of the EOS parameters

The cold compression parameters were calculated in the first step. The molar volume, bulk modulus and derivative bulk modulus in the reference condition were determined by the use of room-temperature compression data. In the present paper, V_0, B_0, and B_0' were calculated based on room-temperature isostatic compression data, but shock-wave data up to almost 500 GPa are presented for comparison. The Einstein characteristic temperature θ_0 is the adjustable parameter of the equation and the other ambient condition parameters (i.e., γ_0 and δ_0) were calculated based on it. Brosh et al. [10] used the constant value of 300 K for simple elements and 500 K for more complex compounds. Since the high-temperature thermal expansion is influenced by some other terms like the anharmonic effect [22], using a lower value of the Einstein temperature eliminated the overestimation and helped to calculate more accurate parameters [23]. On the other hand, most of the transition metals, which are discussed here, are diamagnetic and paramagnetic metals; hence, electronic and magnetic contributions to the specific heat in the temperature below 300 K are negligible. We found that using the actual Einstein temperature could be more beneficial for extreme condition behavior. In this way, the Einstein temperatures of the elements were calculated based on the low-temperature volumetric heat capacity [24]. For simplicity, the Debye temperature [25] or the Einstein temperature calculated from the Debye temperature [24], can also be used as θ_0. The Grüneisen parameter and the Anderson–Grüneisen parameter are determined based on thermal expansion and bulk modulus data at a temperature slightly above θ_0. b_0 is assumed to be 1 for all materials. The high-temperature EOS parameters (i.e., δ_1 and b_1) were calculated based on high-temperature thermal expansion and bulk modulus data by simultaneously solving Eqs. (10) and (12). In some cases, such as vanadium, to our knowledge, high-temperature bulk modulus data are not available, so b_1 is assumed to be 1 and δ_1 is adjusted by the use of the high-temperature thermal expansion value. All calculated parameters are shown in Table 1.

Calculated parameters are used as the input data for ChemSage [26] software to reproduce all thermodynamic properties.

4. Results

4.1. Groups VB and VIB

The body-centered cubic (BCC) transition metals (i.e., molybdenum (Mo), tantalum (Ta), tungsten (W), niobium (Nb), and vanadium (V)) are especially interesting, because they have very high melting points at ambient pressure and, in addition, at room temperature they remain in a stable BCC structure up to extremely high pressures (i.e., tungsten up to 378 GPa [27], molybdenum 416 GPa [27], tantalum 170 GPa [28], niobium 134 GPa [29], and vanadium 69 GPa [30,31]). Total energy calculations for W by Moriarty [32] predict the BCC structure to be stable to 1250 GPa at room temperature and at about 11 000 K at ambient pressure. These make tungsten an appropriate target for high-pressure and high-temperature studies. Because of tungsten's technological importance, strong X-ray diffraction signal and high yield strength, it has been chosen for several studies, and has been widely examined in dynamic and static compression experiments.

The heat capacity [33–36], bulk modulus [7,37–44], molar volume, and thermal expansion [45–54,17,55] of group VB and group VIB elements have been measured many times; a complete review of the thermal expansion experimental data is provided by Wang et al. [55] and Lu et al. [13]. Because of the enormous number of thermal expansion experiments of early transition elements and the diversity of their results, as can be seen in Figs. 2 and 3, it is impossible to develop a model to be consistent with all the data. Hence the experimental data from Touloukian et al. [53] and Wang et al. [55] have been chosen to be the source for volumetric data calculation and comparison. Even though those data are also different from each other, like in the case of Ta, this is the best way that we can control the model. Predictions of the molar volume and bulk modulus with the proposed EOS and Dorogokupets et al.'s [18] semi-empirical EOS as well as their experimental data are shown in Figs. 2 and 3. One of the important limitations of the proposed model is the overestimation of the bulk modulus at high temperatures to avoid mechanical instability at high temperature [10]. As can be seen, the calculated bulk modulus crosses over the experimental data at high temperature, and overestimates the modulus for all elements. On the other hand, for Mo and W and other early transition elements, the anharmonic contributions to entropy are higher than Cu, Ag, and Au [56,57]. Because of that, the high-temperature predicted molar volume data for Mo and Nb have about 3% error in comparison with experimental data. Explicit modeling of anharmonicity can be introduced to the model for better correlation. The experimental volumetric data for V and Ta have about 10% diversity at high temperature. While the calculated data are consistent with the data from Wang et al. [55], the values are about 1.5% lower than for the data from Touloukian et al. [53]. The calculated bulk modulus and molar volume with the Birch–Murnaghan EOS (B–M EOS) [7,17] and the semi-empirical EOS [18] are also shown in Fig. 3. As can be seen, Dorogokupets et al.'s [18] EOS underestimates the bulk modulus of Ta and W and overestimates the data at high temperature. In contrast, the B–M EOS data are almost identical to the experimental data, which can be attributed to the polynomial nature of B–M EOS. However, as shown in Fig. 1, the high-pressure heat capacity calculated with this method becomes negative, but the heat capacity obtained in the present work is almost identical with the calculated heat capacity obtained using Dorogokupets et al.'s [18] EOS. As mentioned before, the high-temperature bulk modulus data are not available for vanadium, but it can be seen that the calculated δ_1 is good enough to predict the thermal expansion data.

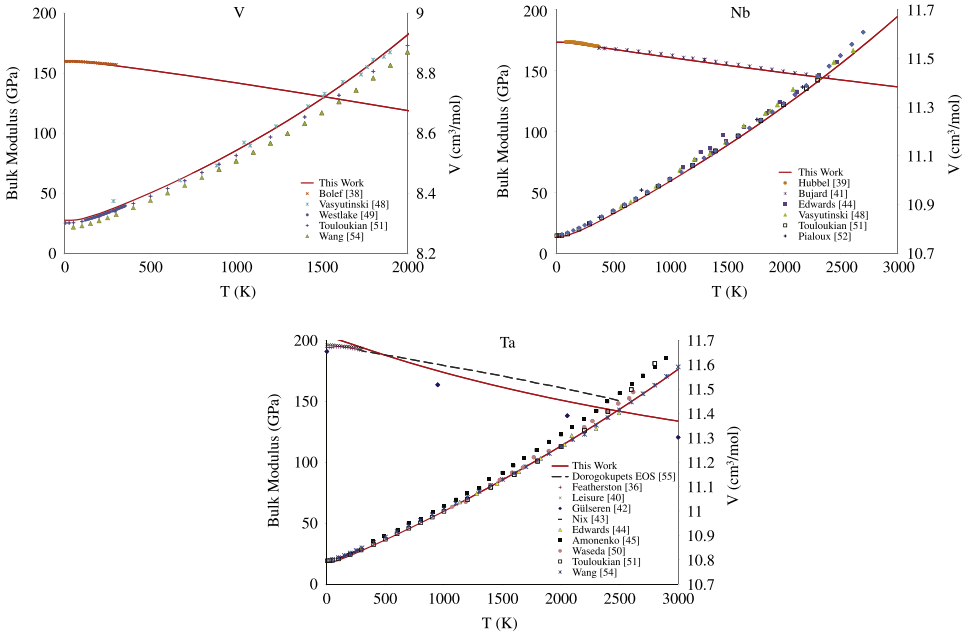

Fig. 2. Calculated molar volume and bulk modulus from this work for V, Nb, and Ta. Calculated bulk modulus data from Dorogokupets et al. [18] and experimental data [37, 40–47,50–55].

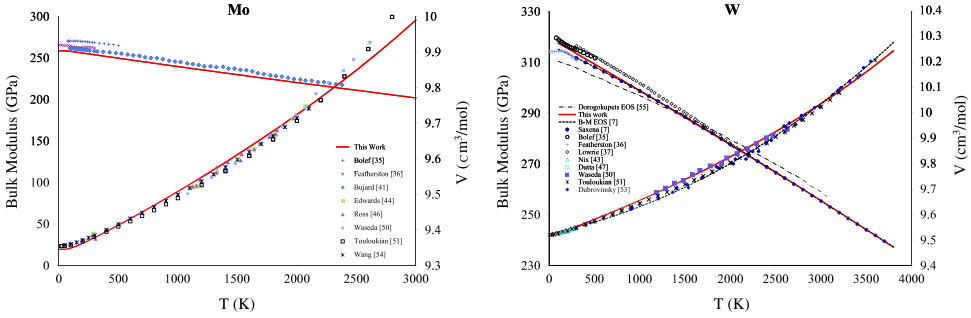

Fig. 3. Calculated molar volume and bulk modulus from this work for Mo and W. Calculated bulk modulus data from Dorogokupets et al. [18], molar volume and bulk modulus from the Birch–Murnaghan EOS (B–M EOS) [7,17] and experimental data [7,37–39,43,45,46,48,49,52,43,17,55] are also shown.

Despite a large number of experimental and theoretical efforts [58–79], agreement on the melting behavior of Mo, Ta, and W at high pressure has been elusive. The first shock wave experiment on high-pressure melting of Mo was done by Hixon et al. [67] up to 350 GPa, followed by early work of Moriarty [70] that employed a many-body total energy function to predict the high-pressure melting curve of Mo. Debates about the melting curve of early transition metals (i.e., groups VA and VIA of the periodic table) started with the work of Errandonea et al. [59] for DAC (Diamond Anvil Cell) high-pressure melting experiments. The DAC data show a low melting slope $dT_m/dP \approx 0$ and its extrapolation up to 350 GPa gives a melting temperature about 4000 K, which is far below the shock wave data value (e.g., $P \approx 380$ GPa, $T_m \approx 1000$ K). Mo is unique, because it has been examined extensively due to having the smallest measured melting slope of that group, thus providing the most severe test. While Ta and W have been less fully examined by shock experiments, they appear to have many of the same features as Mo. The fact that unusually low melting slopes have also been found in the early transition metals Ta, W, Cr, and V indicates that the present results are a general feature of the early transition metals and are not confined to Mo. Theoretical work [70,71,74,75,78] based directly or indirectly on density functional theory (DFT) generally supports the shock data. While Moriarty's [70] calculation overestimates the shock wave experiment data, Belonoshko et al.'s [71] dislocation-mediated melting model underestimates the results. Cazorla et al. [74, 75] used an *ab initio* technique using DFT with simulations of coexisting solid and liquid and calculated the melting curve, which is consistent with shock data. They found out that Mo melts at high pressure at $P \approx 380$ GPa and $T_m \approx 8650$ K, which is in a good agreement with recent experimental shock wave data [69], $P \approx 3740$ GPa and $T_m \approx 7853 \pm 813$ K.

Ross et al. [62] argue that a change of coordination on going from BCC solid to liquid leads to a change of electronic structure, and hence a change in the electron distribution between s–p and d states, and that this redistribution stabilizes the liquid and lowers T_m. Errandonea [63] argues that *ab initio* calculations neglect the rearranging of the electronic structure upon melting, and that this may be a possible cause for the high melting temperatures obtained from *ab initio* calculations, since these calculations do not take into account the free-energy changes produced by alterations of the d-electron band. Ross et al. [62] used a semi-empirical model in which the d-band contribution to the total binding energy is described by the Friedel equation, and showed that omission of the d-band contribution results in a large overestimation of the melting slope of BCC transition metals. The melting curve obtained using that model satisfactorily agrees with the vacancy model estimates and the DAC measurements [63]. Santamaría-Pérez et al. [66] used static DAC measurements and Poisson ratios

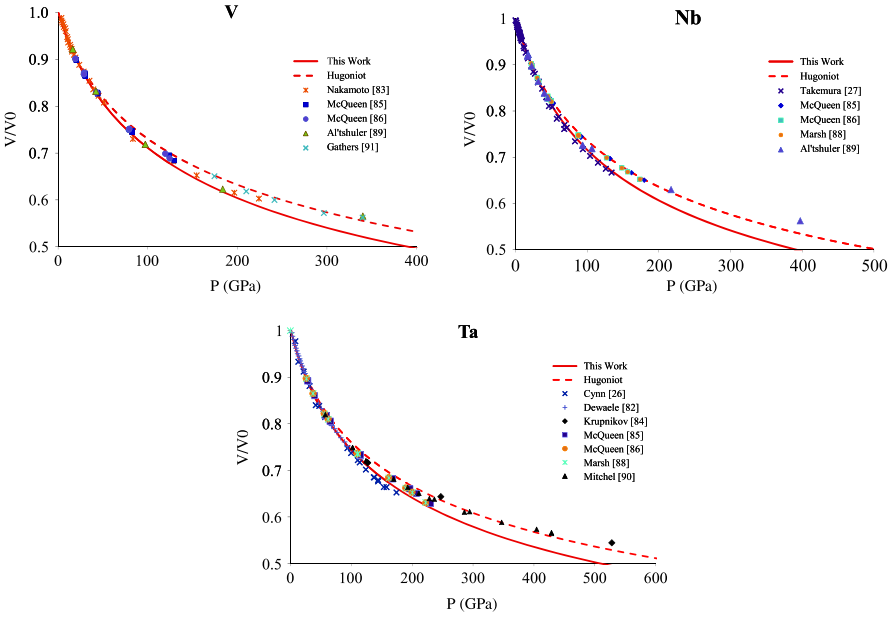

Fig. 4. Calculated cold compression and Hugoniot curves for V, Nb, and Ta as well as their experimental data [28,29,82–86,88–91].

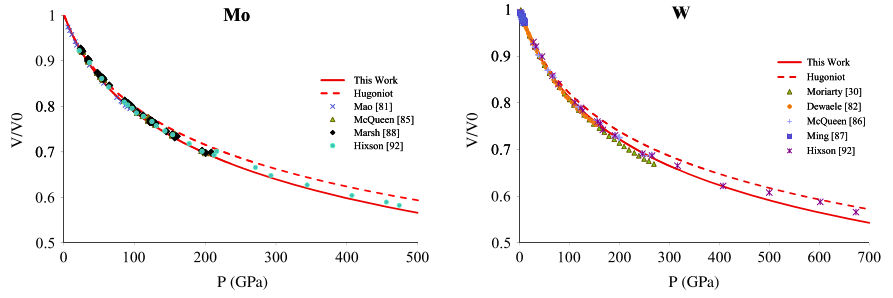

Fig. 5. Calculated cold compression and Hugoniot curves for Mo and W as well as their experimental data [32,81,82,85–88,92].

from shock experiments [67], and proposed a new phase diagram for Mo. In this diagram, the BCC phase extends at 3250 K to 150 GPa, the pressure at which a transition from BCC to a new noncrystalline phase happens, possibly close to the A15 structure. The A15 structure is known to compete favorably with the BCC structure, for the early transition elements Mo, Nb, Ta, and W [80]. Above 150 GPa, the melt is a solid–liquid mixture bounded roughly by a transition region extending from 150 (4100 K) to 390 GPa (∼10 000 K). On the other hand, Cazorla et al. [74] considered all the s–p to d electron transfer effects and changes of d bandwidth in their simulations, and showed that there are only minor changes of both atomic and electronic structure in going from the high-temperature BCC solid to the melt and that the transfer of electrons from s–p states to d states appears to be incompatible with the present DFT calculations. The low melting slope in Ross et al.'s [62] calculation could be due to their perfect crystal assumption of high-temperature solid and the liquid. Cazorla et al. [75] also showed that the BCC crystal structure is the most favored up to 350 GPa (∼8650 K). Disagreements with DAC measurements on Mo and other transition metals are a cause for concern. A major disagreement between DFT predictions and experimental data suggests an unexpected failure either of the commonly used DFT approximations or of apparently well-established experimental techniques. This paper focuses on the high-pressure EOS of the solid materials, but an extension of such an EOS to the liquid state and calculation of the high-pressure melting curve of the elements could be helpful for understanding the melting behavior of the early transition elements and the conflict between DFT results and experimental data.

The room-temperature compression and calculated Hugoniot curves are shown in Figs. 4 and 5. As can be seen, the calculated isotherms are consistent with static compression experimental data [28,29,81–83]. The calculated Hugoniot curves for Nb and Ta are 3% lower than the shock wave data [32,84–92]. This can be attributed to the nature of shock wave experiments; Holzapfel [93] shows that only the fitted equation without any physical meaning can express the reduced shock wave data completely.

The P–V isotherm for Ta, Mo, and W at 1000 K, based on the proposed calculation and data from [92,94], are shown in Fig. 6. Experimental data [95,96] for Mo at 1673 K and its calculated P–V curve is also shown in Fig. 7. Even though the proposed model overestimates the volume at high pressure ($P > 200$ GPa) by about 1% in comparison to other models, the calculated isotherm of Mo at 1673 K is almost identical with the experimental data. The calculated isotherm at 3000 K (not show here) also follows the same pattern for W and Ta.

4.2. Group VIIIB

The low-temperature heat capacity data of platinum and palladium were obtained from [102–106] and recommended values for the their thermal expansion were gathered form [46,49,53,107–110]. High-temperature elastic data are not widely available for Pt and Pd. Data from Rayne [111], Weinmann et al. [112], and Collard et al. [113] are used for calculating the EOS parameters. The low-temperature ($T < 100$ K) bulk modulus data of palladium have some anomalies, as shown in Fig. 8, which can

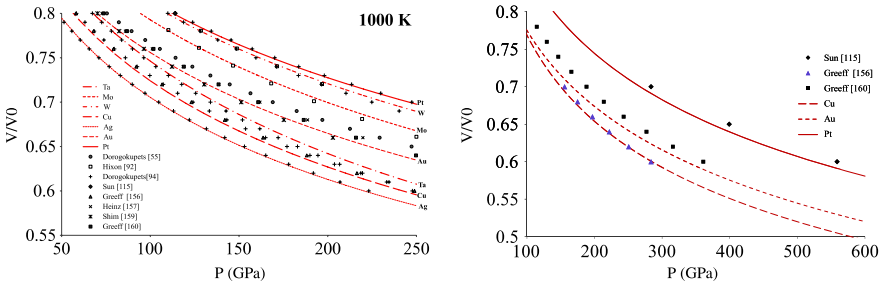

Fig. 6. Calculated isotherm for various elements. (a) 1000 K isotherm for Ta, Mo, W, Cu, Ag, Au, and Pt. (b) 5000 K isotherm for Cu, Au, and Pt. Calculated data from [18,92,94,97–101] are also presented for comparison.

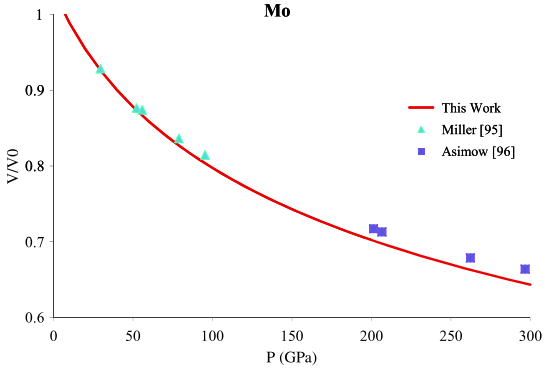

Fig. 7. Comparison of calculated isotherm of Mo at 1674 K with experimental data [95,96].

be attributed to the change with temperature of the contribution to the shear constants, resulting from the holes in the 4d band of palladium [111]. The results of volumetric thermal expansion and bulk modulus are shown in Fig. 8. The calculated results are completely consistent with experimental data for both platinum and palladium.

Platinum and palladium have a face-centered cubic (FCC) crystal structure and do not undergo any phase changes between absolute zero and their melting points. Theoretical calculations [114–116] and experimental results [117] also confirmed the stability of the FCC crystal structure at high pressure. Although platinum is a widely used high-pressure standard due to its chemical inertness and large isothermal compressibility, there has not been a lot of attention paid to palladium.

The room-temperature EOS for Pt is established by reducing the shock Hugoniot and *ab initio* LMTO up to 660 GPa [86,118,119]. However, the EOS developed by Holmes et al. [119] showed some discrepancy in the results, as Dewaele et al. [82] found Holmes et al.'s EOS to overestimate the pressure by ≈4 GPa near 100 GPa at room temperature. Sun et al. [97] found that their room-temperature isotherm is almost identical with that of Holmes et al., below 70 GPa. At high pressures ($P > 200$ GPa), Holmes et al. [119] overestimate the results by about 3% at 200 GPa and systematically increase the error with increasing pressure. Fig. 9 shows the calculated cold compression and Hugoniot curves of palladium and platinum as well as the experimental results. As can be seen, the calculated cold compression curve is identical to that of Dewaele et al. [82], but the Hugoniot curve is about 5% lower than the high-pressure shock wave data [118,119] at 500 GPa. In the case of Pd, the cold compression and Hugoniot curves are almost identical to the experimental data.

Besides the room-temperature isotherm, accurate thermal pressure (P_{th}) data are needed to calibrate the pressure in

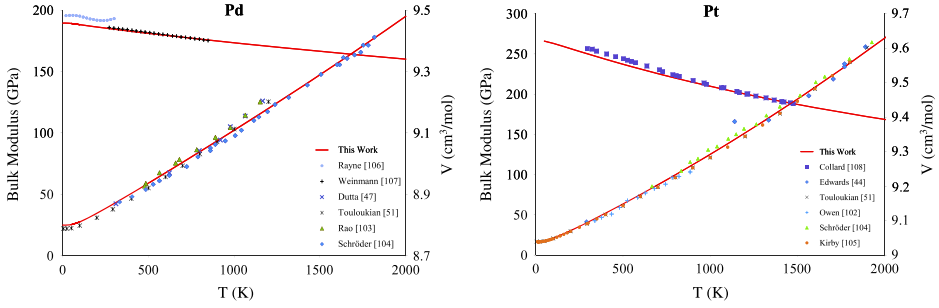

Fig. 8. Calculated and experimental data of molar volume and bulk modulus for Pd and Pt. Experimental data from [46,49,53,107–113].

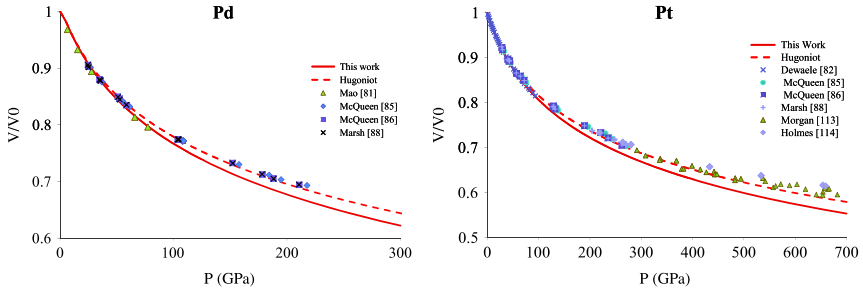

Fig. 9. Calculated cold compression and Hugoniot curves for Pd and Pt as well as their experimental data [81,82,85,86,88,118,119].

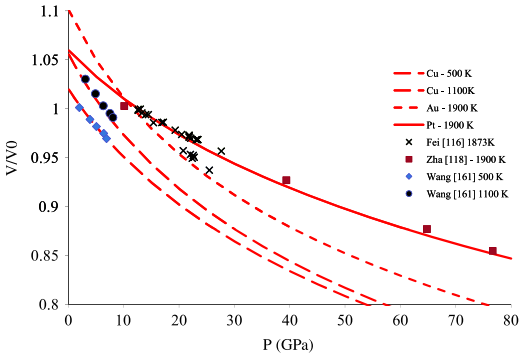

Fig. 10. Comparison of calculated isotherm of Cu at 500 and 1100 K, Au at 1900 K, and Pt at 1900 K with experimental data [120,122,123].

simultaneous high-pressure and high-temperature experiments. P_{th} cannot be easily determined experimentally in the wide range of temperature and volume; so a theoretical approach combined with the experimental data is the best way to construct a thermal EOS for temperature–pressure calibration [120–122]. A comparison of the high-temperature compression of platinum with experimental data and the theoretical calculation is shown in Fig. 6. The calculated data based on the proposed EOS is identical with the DFT calculation [97] and the semi-empirical EOS [94] up to 5000 K. In addition, the calculated 1900 K isotherm shown in Fig. 10 is also consistent with experimental data [120,122].

4.3. Group IB

Copper, silver and gold are in the same column of periodic table; each of them possesses one s-orbital electron on top of a full electron shell. This similarity in electronic configuration endows these metals with similar physical properties such as remarkable electrical conductivity. The EOS parameters for Cu, Ag, and Au are gathered from [34,45,53,81,85,86,90,106,107, 124–149]. Comparisons of the experimental volumetric thermal expansion and bulk modulus data for different temperatures and theoretical predictions from the proposed EOS, the semi-empirical EOS of Dorogokupets et al. [18] and the Debye–Grüneisen model of Lu et al. [13] are shown in Fig. 11. It can be seen that the present model successfully predicts the experimental data. In the case of Cu, the model proposed by Lu et al. [13] underestimates the volume at temperatures lower than 100 K, but has better consistency with the experimental results at high temperatures. On the other hand, both sets of calculated data [13,18] have better correlation with the low-temperature bulk modulus experimental data, while they overestimate the data at high temperature, where proposed model has better consistency. The calculated bulk modulus of silver is about 3% lower than the experimental value in the low-temperature region. This can be attributed to the experimental error, but further experimental data are needed to confirm that.

One of the first high-pressure melting experiments on Cu, Ag, and Au was done by Cohen et al. [150], up to 4 GPa, and this was followed by the work of Mitra et al. [151], who extended the range to 7 GPa for platinum as well as copper, gold, and silver. The most recent melting experiments were done by Errandonea [152], up to 12 GPa. The electronic configuration of Cu, Ag, and Au suggests that their behavior is quite like that of noble gases and follows the same trend, showing a very steep melting curve. The similarities in properties of group IB elements have led the experimental investigations to focus more on Cu as a model [153–155]. In contrast to the case for early transition elements (i.e., Mo, Ta and W), the DAC and shock wave melting experiments are in good agreement with the theoretical calculation. However, there is a slight temperature offset between the calculated values and the experimental values, due to technical difficulties of experiments and the inherent error associated with the calculations [72,116, 156–158]. Agreement between DFT results and experimental data can be a good source of reliable data for testing the high-pressure EOS for calculating the melting curve of the group IB elements.

Cu and Au remain in an FCC structure up to pressures higher than 100 GPa. While Ahuja et al. [159] predict the phase transformation in gold at room temperature to be at about 240 GPa, Söderlind [160] argued that the only transformation in gold occurs at about 2 TPa. Theoretical calculation of the electronic structure of Cu [98] also does not show any phase transformation up to quite high pressure. The high-pressure crystal stability of Cu and Au make them good candidates for high-pressure calibration standards, and several mathematical EOSs

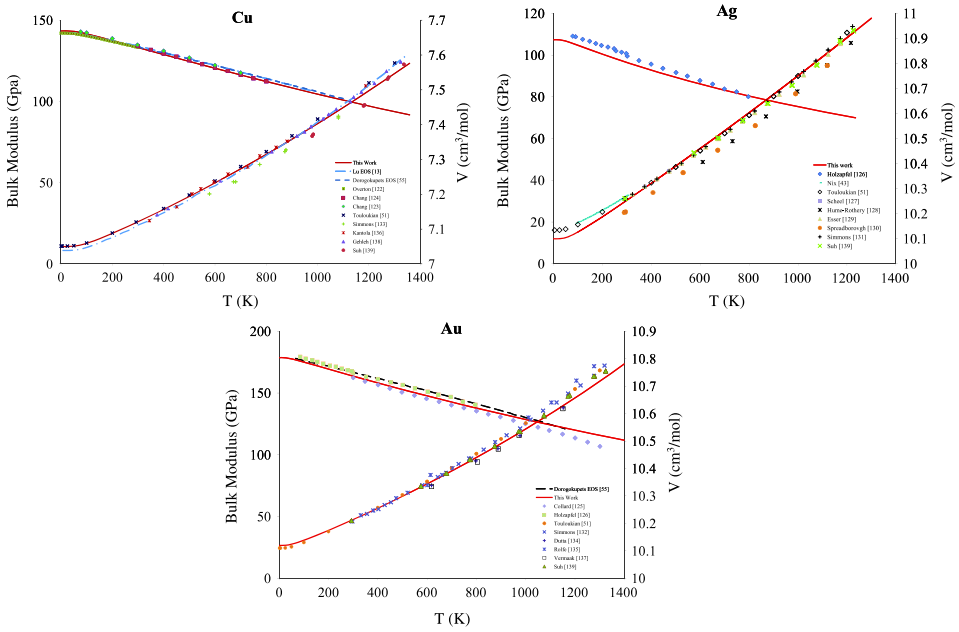

Fig. 11. Calculated molar volume and bulk modulus from this work for Cu, Ag, and Au. Calculated bulk modulus data from Dorogokupets et al. [18], molar volume, and bulk modulus form Lu et al. EOS (Lu EOS) [13] and experimental data [45,53,127–144] are also shown.

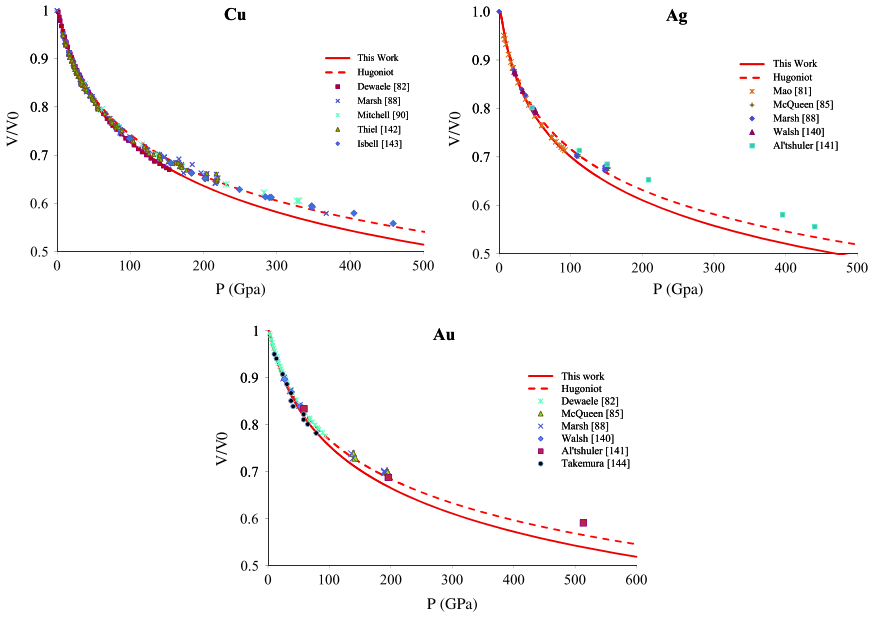

Fig. 12. Calculated cold compression and Hugoniot curves for Cu, Ag, and Au as well as their experimental data [81,82,85,88,90,145–149].

have been formulated [98,99,161,100,101] to predict their *PVT* behavior. High-pressure isotherms for Cu, Ag, and Au from the present EOS and other calculated and experimental data [18,94, 120,98,123] are shown in Figs. 6 and 10. It is clear that theoretical prediction of the present EOS is almost identical to the data of Dorogokupets et al. [94] and Greeff et al. [98] for Cu and Ag, but the calculated data for Au are lower than other calculated data except for Shim et al.'s [100]. While Dorogokupets et al.'s [18] data are obviously higher than those of other models [99–101], the difference between the presented model and data from Greef et al. [101] decreases with increasing pressure, and the values are almost identical at 5000 K and 300 GPa.

The room-temperature compression and Hugoniot data up to 500 GPa are also shown in Fig. 12. The calculated cold compression and Hugoniot curves completely follow the experimental data up to 200 GPa. Above that there is about 5% error between the calculated Hugoniot curve and the shock wave experiment data. Holzapfel [162] recently showed that in the shock wave data of Cu, Ag, and Au, typically 2–5% lower pressure is seen for almost all shock wave reduced isotherms at 200 GPa. He argued that the shock-compressed solid just before melting may be strongly disordered, with disorder entropy similar to the entropy of melting, and that this can cause some discrepancy in high-pressure data.

5. Conclusion

The so-called explicit Gibbs free energy EOS was used to calculate the high-pressure properties of several elements, based on CALPHAD methodology. The proposed EOS uses an interpolation with a Thomas–Fermi model and do not show any negative value for heat capacity. The EOS parameter was calculated for ten BCC and FCC transition elements, and the results show good agreement with different experimental data. High-pressure shock wave data show a major discrepancy with calculated Hugoniot results, but this may be due to uncertainty and lack of accuracy of the shock wave data at high pressure.

Appendix. Supplementary data

Supplementary material related to this article can be found online at doi:10.1016/j.calphad.2010.11.007.

References

[1] H. Lukas, S.G. Fries, B. Sundman, Computational Thermodynamics: The CALPHAD Method, Cambridge University Press, New York, NY, USA, 2007.
[2] L.E. Fried, W.M. Howard, Explicit Gibbs free energy equation of state applied to the carbon phase diagram, Phys. Rev. B 61 (13) (2000) 8734–8743.
[3] A.F. Guillermet, P. Gustafson, M. Hillert, The representation of thermodynamic properties at high pressures, J. Phys. Chem. Solids. 46 (12) (1985) 1427–1429.
[4] P. Vinet, J. Ferrante, J.R. Smith, J.H. Rose, A universal equation of state for solids, J. Phys. C: Solid State Phys. 19 (1986) L467–L473.
[5] P. Vinet, J.H. Rose, J. Ferrante, J.R. Smith, Universal features of the equation of state of solids, J. Phys.: Condens. Matter 1 (1989) 1941–1963.
[6] S.K. Saxena, Earth mineralogical model: Gibbs free energy minimization computation in the system MgO–FeO–SiO_2, Geochim Cosmochim Acta. 60 (13) (1996) 2379–2395.
[7] S.K. Saxena, J. Zhang, Thermochemical and pressure–volume–temperature systematics of data on solids, examples: tungsten and MgO, Phys. Chem. Miner. 17 (1) (1990) 45–51.
[8] O.L. Anderson, Equations of State of Solids for Geophysics and Ceramic Science, Oxford University Press, USA, 1995.
[9] M.H.G. Jacobs, H.A.J. Oonk, A realistic equation of state for solids. The high pressure and high temperature thermodynamic properties of MGO, CALPHAD 24 (2) (2000) 133–147.
[10] E. Brosh, G. Makov, R.Z. Shneck, Application of CALPHAD to high pressures, CALPHAD 31 (2) (2007) 173–185.
[11] E. Brosh, R.Z. Shneck, G. Makov, Explicit Gibbs free energy equation of state for solids, J. Phys. Chem. Solids. 69 (8) (2008) 1912–1922.
[12] X.-G. Lu, M. Selleby, B. Sundman, Implementation of a new model for pressure dependence of condensed phases in Thermo-Calc, CALPHAD 29 (1) (2005) 49–55.
[13] X.-G Lu, Q. Chen, A CALPHAD Helmholtz energy approach to calculate thermodynamic and thermophysical properties of fcc Cu, PMag. 89 (25) (2009) 2167.
[14] X.-G. Lu, M. Selleby, B. Sundman, Theoretical modeling of molar volume and thermal expansion, Acta Mater. 53 (8) (2005) 2259–2272.
[15] X.-G. Lu, M. Selleby, B. Sundman, Assessments of molar volume and thermal expansion for selected bcc, fcc and hcp metallic elements, CALPHAD 29 (1) (2005) 68–89.
[16] X.-G. Lu, M. Selleby, B. Sundman, Calculations of thermophysical properties of cubic carbides and nitrides using the Debye–Grüneisen model, Acta Mater. 55 (4) (2007) 1215–1226.
[17] L.S. Dubrovinsky, S.K. Saxena, Thermal expansion of periclase (MgO) and Tungsten (W) to melting temperatures, Phys. Chem. Miner. 24 (8) (1997) 547–550.
[18] P.I. Dorogokupets, A.R. Oganov, Ruby, metals, and MgO as alternative pressure scales: a semiempirical description of shock-wave, ultrasonic, X-ray, and thermochemical data at high temperatures and pressures, Phys. Rev. B 75 (2) (2007) 24115.
[19] A.T. Dinsdale, SGTE data for pure elements, CALPHAD 15 (4) (1991) 317–425.
[20] E. Brosh, G. Makov, R.Z. Shneck, Thermodynamic analysis of light-actinide elements. in: Proceedings of the 11th International Symposium on Thermodynamics of Nuclear Materials, vol. 344, issue(1–3), 2005, pp. 36–39.

[21] E. Brosh, G. Makov, R.Z. Shneck, Thermodynamic analysis of high-pressure phase equilibria in Fe–Si alloys, implications for the inner-core, PEPI 172 (3–4) (2009) 289–298.
[22] A.R. Oganov, P.I. Dorogokupets, Intrinsic anharmonicity in equations of state and thermodynamics of solids, J. Phys.: Condens Matter. 16 (2004) 1351–1360.
[23] E. Brosh, Personal Communication, 2009.
[24] L.A. Girifalco, Statistical Mechanics of Solids, Oxford University Press, USA, 2000.
[25] C. Kittel, P. McEuen, Introduction to Solid State Physics, Wiley, New York, 1996.
[26] G. Eriksson, K. Hack, ChemSage — a computer program for the calculation of complex chemical equilibria, Metall. Mater. Trans. B 21 (6) (1990) 1013–1023.
[27] A.L. Ruoff, H. Xia, H. Luo, Y.K. Vohra, Miniaturization techniques for obtaining static pressures comparable to the pressure at the center of the earth: X-ray diffraction at 416 GPa, Rev. Sci. Instrum. 61 (1990) 3830.
[28] H. Cynn, C.S. Yoo, Equation of state of Tantalum to 174 GPa, Phys. Rev. B 59 (13) (1999) 8526–8529.
[29] K. Takemura, A.K. Singh, High-pressure equation of state for Nb with a helium-pressure medium: powder X-ray diffraction experiments, Phys. Rev. B 73 (2006) 224119–224128.
[30] Y. Ding, R. Ahuja, J. Shu, P. Chow, W. Luo, H. Mao, Structural phase transition of vanadium at 69 GPa, Phys. Rev. Lett. 98 (8) (2007) 85502.
[31] A.K. Verma, P. Modak, Structural phase transitions in Vanadium under high pressure, Europhys. Lett. 81 (2008) 37003.
[32] J.A. Moriarty, Ultrahigh-pressure structural phase transitions in Cr, Mo, and W, Phys. Rev. B 45 (5) (1992) 2004–2014.
[33] C.T. Anderson, The heat capacities of vanadium, vanadium trioxide, vanadium tetroxide and vanadium pentoxide at low temperatures 1, JACS 58 (4) (1936) 564–566.
[34] G.K. White, S.J. Colloco, Heat capacity of reference materials: Cu and W, J. Phys. Chem. Ref. Data. 13 (4) (1984).
[35] A.F. Guillermet, Critical evaluation of the thermodynamic properties of Molybdenum, Int. J. Thermophys. 6 (4) (1985) 367–393.
[36] Y. Takahashi, J. Nakamura, The heat capacity of tantalum from 80 to 1000 K, Thermochim. Acta. 282 (1996) 317–322.
[37] D.I. Bolef, J. De Klerk, Elastic constants of single-crystal Mo and W between 77 and 500 K, J. Appl. Phys. 33 (1962) 2311–2314.
[38] F.H. Featherston, J.R. Neighbours, Elastic constants of tantalum, tungsten, and molybdenum, Phys. Rev. 130 (4) (1963) 1324–1333.
[39] R. Lowrie, A.M. Gonas, Single-crystal elastic properties of Tungsten from 24 to 1800 °C, J. Appl. Phys. 38 (11) (1967) 4505–4509.
[40] D.I. Bolef, R.E. Smith, J.G. Miller, Elastic properties of vanadium. I. Temperature dependence of the elastic constants and the thermal expansion, Phys. Rev. B 3 (12) (1971) 4100–4108.
[41] W.C. Hubbell, F.R. Brotzen, Elastic constants of niobium–molybdenum alloys in the temperature range −190 to +100 °C, J. Appl. Phys. 43 (1972) 3306.
[42] R.G. Leisure, D.K. Hsu, B.A. Seiber, Elastic properties of tantalum over the temperature range 4300 K, J. Appl. Phys. 44 (1973) 3394.
[43] P. Bujard, R. Sanjines, E. Walker, J. Ashkenazi, M. Peter, Elastic constants in Nb–Mo alloys from zero temperature to the melting point: experiment and theory, J. Phys. F: Metal Phys. 11 (1981) 775–786.
[44] O. Gülseren, R.E. Cohen, High-pressure thermoelasticity of body-centered-cubic tantalum, Phys. Rev. B 65 (6) (2002) 64103.
[45] F.C. Nix, D. MacNair, The thermal expansion of pure metals. II: molybdenum, palladium, silver, tantalum, tungsten, platinum, and lead, Phys. Rev. 61 (1–2) (1942) 74–78.
[46] J.W. Edwards, R. Speiser, H.L. Johnston, High temperature structure and thermal expansion of some metals as determined by X-ray diffraction data. I. Platinum, tantalum, niobium, and molybdenum, J. Appl. Phys. 22 (1951) 424.
[47] V.M. Amonenko, B.M. Vasyutinskii, G.N. Kartmazov, Y.N. Smirnov, V.A. Finkel, Tantalum structure at elevated temperature, Fiz. Met. Metalloved. (1963) 15.
[48] R.G. Ross, W. Hume-Rothery, High temperature X-ray metallography, J. Less Common. Metals 5 (3) (1963) 258.
[49] B.N. Dutta, B. Dayal, Lattice constants and thermal expansion of palladium and tungsten up to 878 °C by X-ray method, Phys. Status Solidi B: Basic Solid State Phys. 3 (12) (1963) 2253–2259.
[50] B.M. Vasyutinskii, G.N. Kartmazov, Y.N. Smirnov, V.A. Finkel, Niobium and vanadium crystal structure at high temperature, Phys. Metals Metallogr. 21 (1966) 134.
[51] D.G. Westlake, S.T. Ockers, Thermal expansion of Vanadium and Vanadium hydride at low temperature, J. Less Common. Metals 22 (2) (1970) 225–230.
[52] Y. Waseda, K. Hirata, M. Ohtani, High-temperature thermal expansion of Pt, Ta, Mo and W measured by X-ray diffraction, High Temp. - High Press. 7 (2) (1975) 221–226.
[53] Y.S. Touloukian, R.K. Kirby, R.E. Taylor, P.D. Desai, Thermophysical properties of matter, volume 12: thermal expansion, Metal. Elements Alloys (1979).
[54] A. Pialoux, M.L. Joyeux, G. Cizeron, Étude du comportement du Niobium sous vide par diffraction des rayons X à haute température, J. Less Common Metals 87 (1) (1982) 1–19.
[55] K. Wang, R.R. Reeber, The role of defects on thermophysical properties: thermal expansion of V, Nb, Ta, Mo and W, Mater. Sci. Eng.: R: Rep. 23 (3) (1998) 101–137.
[56] A.F. Guillermet, G. Grimvall, Analysis of thermodynamic properties of Molybdenum and Tungsten at high temperatures, Phys. Rev. B 44 (9) (1991) 4332–4340.
[57] D.C. Wallace, Statistical mechanics of monatomic liquids, Phys. Rev. E 56 (4) (1997) 4179.
[58] N.S. Fateeva, L.F. Vereshchagin, Melting curve of Molybdenum up to 90 kbar, JETP Lett. 14 (4) (1971) 153–154.
[59] D. Errandonea, B. Schwager, R. Ditz, C. Gessmann, R. Boehler, M. Ross, Systematics of transition-metal melting, Phys. Rev. B 63 (13) (2001) 132104.
[60] D. Errandonea, M. Somayazulu, D. Häusermann, H.K. Mao, Melting of Tantalum at high pressure determined by angle dispersive X-ray diffraction in a double-sided laser-heated diamond-anvil cell, J. Phys: Condens Matter 15 (45) (2003) 7635.
[61] D. Errandonea, Comment on 'theoretical solid and liquid state shock Hugoniots of Al, Ta, Mo and W', J. Phys: Condens Matter. 16 (47) (2004) 8801.
[62] M. Ross, L.H. Yang, R. Boehler, Melting of aluminum, molybdenum, and the light actinides, Phys. Rev. B 70 (18) (2004) 184112.
[63] D. Errandonea, Improving the understanding of the melting behaviour of Mo, Ta, and W at extreme pressures, Phys. B: Condens. Matter 357 (3–4) (2005) 356–364.
[64] D. Errandonea, Phase behavior of metals at very high PT conditions: a review of recent experimental studies, J. Phys. Chem. Solids. 67 (9–10) (2006) 2017–2026.
[65] M. Ross, R. Boehler, D. Errandonea, Melting of transition metals at high pressure and the influence of liquid frustration: the late metals Cu, Ni, and Fe, Phys. Rev. B 76 (18) (2007) 184117.
[66] D. Santamaria-Perez, M. Ross, D. Errandonea, G.D. Mukherjee, M. Mezouar, R. Boehler, X-ray diffraction measurements of Mo melting to 119 GPa and the high pressure phase diagram, J. Chem. Phys. 130 (12) (2009) 124509-8.
[67] R.S. Hixson, D.A. Boness, J.W. Shaner, J.A. Moriarty, Acoustic velocities and phase transitions in Molybdenum under strong shock compression, Phys. Rev. Lett. 62 (6) (1989) 637–640.
[68] X. Zhang, Z. Liu, Y. Gu, L. Cai, F. Jing, Temperature in Molybdenum at high shock pressure: experiment and theory, Phys. B: Condens. Matter. 403 (18) (2008) 3261–3265.
[69] Z. Xiu-Lu, et al., Melting behaviour of Mo by shock wave experiment, Chinese Phys. Lett. 25 (8) (2008) 2969.
[70] J.A. Moriarty, Angular forces and melting in bcc transition metals: a case study of Molybdenum, Phys. Rev. B 49 (18) (1994) 12431–12445.
[71] A.B. Belonoshko, S.I. Simak, A.E. Kochetov, B. Johansson, L. Burakovsky, D.L. Preston, High-pressure melting of Molybdenum, Phys. Rev. Lett. 92 (19) (2004) 195701.
[72] J.A. Moriarty, et al., Quantum-based atomistic simulation of materials properties in transition metals, J. Phys: Condens Matter. 14 (11) (2002) 2825.
[73] S.N. Luo, D.C. Swift, On high-pressure melting of Tantalum, Phys. B: Condens. Matter. 388 (1–2) (2007) 139–144.
[74] C. Cazorla, M.J. Gillan, S. Taioli, D. Alfé, Ab initio melting curve of Molybdenum by the phase coexistence method, J. Chem. Phys. 126 (2007) 194502.
[75] C. Cazorla, M.J. Gillan, S. Taioli, D. Alfé, Melting curve and Hugoniot of Molybdenum up to 400 GPa by ab initio simulations, J. Phys.: Conf. Ser. 121 (1) (2008) 012009.
[76] Z.-L. Liu, X.-L. Zhang, L.-C. Cai, X.-R. Chen, Q. Wu, F.-Q. Jing, Thermal equation of state, and melting and thermoelastic properties of bcc tantalum from molecular dynamics, J. Phys. Chem. Solids. 69 (11) (2008) 2833–2840.
[77] S. Taioli, C. Cazorla, M.J. Gillan, D. Alfé, Ab-initio melting curve and principal Hugoniot of Tantalum, J. Phys.: Conf. Ser. 121 (1) (2008) 012010.
[78] F. Xi, L. Cai, Theoretical study of melting curves on Ta, Mo, and W at high pressures, Phys. B: Condens. Matter 403 (12) (2008) 2065–2070.
[79] A.K. Verma, et al., Theoretical solid and liquid state shock Hugoniots of Al, Ta, Mo and W, J. Phys: Condens Matter. 16 (28) (2004) 4799.
[80] C. Berne, A. Pasturel, M. Sluiter, B. Vinet, Ab initio study of metastability in refractory metal based systems, Phys. Rev. Lett. 83 (8) (1999) 1621–1623.
[81] H.K. Mao, P.M. Bell, J.W. Shaner, D.J. Steinberg, Specific volume measurements of Cu, Mo, Pd, and Ag and calibration of the ruby R fluorescence pressure gauge from 0.06 to 1 Mbar, J. Appl. Phys. 49 (1978) 3276.
[82] A. Dewaele, P. Loubeyre, M. Mezouar, Equations of state of six metals above 94 GPa, Phys. Rev. B 70 (9) (2004) 94112.
[83] Y. Nakamoto, K. Takemura, M. Ishizuka, K. Shimizu, T. Kikegawa (Eds.) Equation of state for vanadium under hydrostatic conditions, in: Joint 20th AIRAPT – 43th EHPRG, 2005, Karlsruhe, Germany.
[84] K.K. Krupnikov, A.A. Bakanova, M.I. Brazhnik, R.F. Trunin (Eds.), An investigation of the shock compressibility of Titanium, Molybdenum Tantalum, and Iron SPhD, 1963.
[85] R.G. McQueen, S.P. Marsh, Equation of state for nineteen metallic elements from shock-wave measurements to two megabars, J. Appl. Phys. 31 (1960) 1253.
[86] R.G. McQueen, S.P. Marsh, J.W. Taylor, J.N. Fritz, W.J. Carter, The equation of state of solids from shock wave studies, High Velocity Impact Phenom. 294 (1970) 417.
[87] L. Ming, M.H. Manghnani, Isothermal compression of bcc transition metals to 100 kbar, J. Appl. Phys. 49 (1978) 208.
[88] S.P. Marsh, LASL Shock Hugoniot Data, University of California Press, 1980.
[89] L.V. Al'tshuler, A.A. Bakanova, I.P. Dudoladov, E.A. Dynin, R.F. Trunin, B.S. Chekin, Shock adiabats for metals. New data, statistical analysis and general regularities, JAMTP. 22 (1981) 145.

[90] A.C. Mitchell, W.J. Nellis, Shock compression of aluminum, Copper, and Tantalum, J. Appl. Phys. 52 (1981) 3363.
[91] G.R. Gathers, Hugoniot measurements for Vanadium, J. Appl. Phys. 59 (1986) 3291.
[92] R.S. Hixson, J.N. Fritz, Shock compression of Tungsten and Molybdenum, J. Appl. Phys. 71 (1992) 1721.
[93] W.B. Holzapfel (Ed.), Problems in shock wave reduced isotherms, in: Physics of Extreme States of Matter-2010, 2010.
[94] P.I. Dorogokupets, A.R. Oganov (Eds.), Equations of state of Al, Au, Cu, Pt, Ta, and W and revised ruby pressure scale, in: Doklady Earth Sciences, Springer, 2006.
[95] G.H. Miller, T.J. Ahrens, E.M. Stolper, The equation of state of Molybdenum at 1400 C, J. Appl. Phys. 63 (1988) 4469.
[96] P.D. Asimow, D. Sun, T.J. Ahrens, Shock compression of preheated Molybdenum to 300 GPa, PEPI 174 (1–4) (2009) 302–308.
[97] T. Sun, K. Umemoto, Z. Wu, J.-C. Zheng, R.M. Wentzcovitch, Lattice dynamics and thermal equation of state of platinum, Phys. Rev. B 78 (2) (2008) 024304.
[98] C.W. Greeff, J.C. Boettger, M.J. Graf, J.D. Johnson, Theoretical investigation of the Cu EOS standard, J. Phys. Chem. Solids 67 (9–10) (2006) 2033–2040.
[99] D. Heinz, R. Jeanloz, The equation of state of the gold calibration standard, J. Appl. Phys. 55 (4) (1984) 885–893.
[100] S.H. Shim, T.S. Duffy, K. Takemura, Equation of state of Gold and its application to the phase boundaries near 660 km depth in Earth's mantle, Earth Planet Sci. Lett. 203 (2) (2002) 729–739.
[101] C.W. Greeff, M.J. Graf, Lattice dynamics and the high-pressure equation of state of Au, Phys. Rev. B 69 (5) (2004) 054107.
[102] J. Crangle, T.F. Smith, Specific heat of metallic Palladium between 65 and 105 °K, Phys. Rev. Lett. 9 (3) (1962) 86–87.
[103] J.L. Feldman, G.K. Horton, Critical analysis of the thermodynamic data for Pt and a prediction of Θ_{DW}(T), Phys. Rev. 137 (4A) (1965) A1106–A1108.
[104] G.E. Shoemake, J.A. Rayne, Specific heat of platinum from 1.4 to 100 K, Phys. Lett. A. 26 (6) (1968) 222–223.
[105] G.T. Furukawa, M.L. Reilly, J.S. Gallagher, Critical analysis of heat-capacity data and evaluation of thermodynamic properties of ruthenium, rhodium, palladium, iridium, and platinum from 0 to 300 K. A survey of the literature data on Osmium, J. Phys. Chem. Ref. Data. 3 (1) (1974).
[106] J. Rupp, R. Birringer, Enhanced specific-heat-capacity (cp) measurements (150–300 K) of nanometer-sized crystalline materials, Phys. Rev. B 36 (15) (1987) 7888–7890.
[107] E.A. Owen, E.L. Yates, Thermal expansion of crystal lattices of silver, platinum and zinc, PMag. 17 (1934) 113–131.
[108] C.N. Rao, K.K. Rao, Effect of temperature on the lattice parameters of some silver–palladium alloys, Can. J. Phys. 42 (7) (1964) 1336–1342.
[109] R.H. Schröder, N. Schmitz-Pranghe, R. Kohlhaas, Experimental determination of the lattice parameters of platinum metals in the temperature range of 190–1709 C, Z. Met.kd 63 (1972) 12–16 (in German).
[110] R.K. Kirby, Platinum, a thermal expansion reference material, Int. J. Thermophys. 12 (4) (1991) 679–685.
[111] J.A. Rayne, Elastic constants of Palladium from 4.2 to 300 K, Phys. Rev. 118 (6) (1960) 1545–1549.
[112] C. Weinmann, S. Steinemann, Lattice and electronic contributions to the elastic constants of Palladium, Solid State Commun. 15 (2) (1974) 281–285.
[113] S.M. Collard, R.B. McLellan, High-temperature elastic constants of platinum single crystals, AcM&M 40 (4) (1992) 699–702.
[114] R. Ahuja, P. Söderlind, J. Trygg, J. Melsen, J.M. Wills, B. Johansson, et al., Influence of pseudocore valence-band hybridization on the crystal-structure phase stabilities of transition metals under extreme compressions, Phys. Rev. B 50 (19) (1994) 14690–14693.
[115] N. Singh, Structural phase transformation of Cu, Pd and Au using transition metal pair potential, Phys. B: Condens. Matter. 269 (2) (1999) 211–220.
[116] J.-W. Jeong, K.J. Chang, Molecular-dynamics simulations for the shock Hugoniot meltings of Cu, Pd and Pt, J. Phys: Condens Matter. 11 (19) (1999) 3799.
[117] A. Kavner, R. Jeanloz, High-pressure melting curve of platinum, J. Appl. Phys. 83 (1998) 7553.
[118] J.A. Morgan, The equation of state of platinum to 680 GPa, High Temperatures–High Pressures 6 (1974) 195–201.
[119] N.C. Holmes, J.A. Moriarty, G.R. Gathers, W.J. Nellis, The equation of state of platinum to 660 GPa (6.6 Mbar), J. Appl. Phys. 66 (7) (1989) 2962–2967.
[120] Y. Fei, J. Li, K. Hirose, W. Minarik, J. Van Orman, C. Sanloup, et al., A critical evaluation of pressure scales at high temperatures by in situ X-ray diffraction measurements, Phys. Earth Planet. Inter. 143–144 (2004) 515–526.
[121] S. Xiang, L. Cai, Y. Bi, F. Jing, S. Wang, Thermal equation of state for Pt, Phys. Rev. B 72 (18) (2005) 184102.
[122] C. Zha, K. Mibe, W. Bassett, O. Tschauner, H. Mao, R. Hemley, PVT equation of state of platinum to 80 GPa and 1900 K from internal resistive heating/X-ray diffraction measurements, J. Appl. Phys. 103 (5) (2008) 4908.
[123] Y. Wang, J. Zhang, H. Xu, Z. Lin, L.L. Daemen, Y. Zhao, et al., Thermal equation of state of Copper studied by high PT synchrotron X-ray diffraction, Appl. Phys. Lett. 94 (2009) 071904.
[124] P.F. Meads, W.R. Forsythe, W.F. Giauque, The heat capacities and entropies of Silver and Lead from 15 to 300 K, JACS 63 (7) (1941) 1902–1905.
[125] W.F. Giauque, P.F. Meads, The heat capacities and entropies of Aluminum and Copper from 15 to 300 K, JACS 63 (7) (1941) 1897–1901.
[126] T.H. Geballe, W.F. Giauque, The heat capacity and entropy of Gold from 15 to 300 K, JACS 74 (9) (1952) 2368–2369.
[127] W.C. Overton, J. Gaffney, Temperature variation of the elastic constants of cubic elements: I. Copper, Phys. Rev. 98 (4) (1955) 969–977.
[128] Y.A. Chang, R. Hultgren, The dilation contribution to the heat capacity of Copper and α-Brass at elevated temperatures, J. Phys. Chem. 69 (12) (1965) 4162–4165.
[129] Y.A. Chang, L. Himmel, Temperature dependence of the elastic constants of Cu, Ag, and Au above room temperature, J. Appl. Phys. 37 (1966) 3567.
[130] S.M. Collard, R.B. McLellan, High-temperature elastic constants of Gold single-crystals, AcM&M 39 (12) (1991) 3143–3151.
[131] W.B. Holzapfel, M. Hartwig, W. Sievers, Equations of state for Cu, Ag, and Au for wide ranges in temperature and pressure up to 500 GPa and above, J. Phys. Chem. Ref. Data. 30 (2) (2001) 515–530.
[132] K. Scheel, About the thermal expansion of some substances. I, Z. Phys. A: Hadrons Nucl. 5 (2) (1921) 167–172 (in German).
[133] W. Hume-Rothery, P.W. Reynolds, A high-temperature Debye–Scherrer camera, and its application to the study of the lattice spacing of Silver, Proc. Roy. Soc. Lond. Ser. A, Math. Phys. Sci. (1938) 25–34.
[134] H. Esser, H. Eusterbrock, Untersuchung der Warmeausdehnung von einigen Metallen und Legierungen mit einem verbesserten Dilatometer, Arch Eisenhüttenw. 14 (7) (1941) 341.
[135] J. Spreadborough, J.W. Christian, High-temperature X-ray diffractometer, J. Sci. Instrum. 36 (1959) 116–118.
[136] R.O. Simmons, R.W. Balluffi, Measurement of the equilibrium concentration of lattice vacancies in Silver near the melting point, Phys. Rev. 119 (2) (1960) 600–605.
[137] R.O. Simmons, R.W. Balluffi, Measurement of equilibrium concentrations of lattice vacancies in Gold, Phys. Rev. 125 (3) (1962) 862–872.
[138] R.O. Simmons, R.W. Balluffi, Measurement of equilibrium concentrations of vacancies in Copper, Phys. Rev. 129 (4) (1963) 1533–1544.
[139] B.N. Dutta, B. Dayal, Lattice constants and thermal expansion of Gold up to 878 °C by X-ray method, Phys. Status Solidi B: Basic Solid State Phys. 3 (3) (1963) 473–477.
[140] C. Rolfe, The lattice parameters of pure Gold, J. Inst. Metals 94 (1966) 148.
[141] M. Kantola, E. Tokola, X-ray studies on the thermal expansion of copper–nickel alloys, Ann. Acad. Sci. Fenn A6: Phys. 223 (1967) 3–11.
[142] J.S. Vermaak, D. Kuhlmann-Wilsdorf, Measurement of the average surface stress of Gold as a function of temperature in the temperature range 50°–985°, J. Phys. Chem. 72 (12) (1968) 4150–4154.
[143] P.C. Gehlen, A 77–1300 K single crystal X-ray specimen chamber, Rev. Sci. Instrum. 40 (1969) 715.
[144] I.K. Suh, H. Ohta, Y. Waseda, High-temperature thermal expansion of six metallic elements measured by dilatation method and X-ray diffraction, J. Mat. Sci. 23 (2) (1988) 757–760.
[145] J.M. Walsh, M.H. Rice, R.G. McQueen, F.L. Yarger, Shock-wave compressions of twenty-seven metals. Equations of state of metals, Phys. Rev. 108 (2) (1957) 196–216.
[146] L.V. Al'tshuler, K.K. Krupnikov, M.I. Brazhnik, Dynamic compressibility of metals under pressures from 400,000 to 4,000,000 atmospheres, SJETP 7 (4) (1958) 614–619.
[147] M.V. Thiel, A.S. Kusubov, Compendium of shock wave data. Report UCRL-50108Livermore: University of California. (1966).
[148] W.H. Isbell, F.H. Shipman, A.H. Jones, Hugoniot equation of state measurements for eleven materials to five megabars: general motors corporation, Material Science Laboratory, Report MSL-68-13. 1968.
[149] K. Takemura, Evaluation of the hydrostaticity of a helium-pressure medium with powder X-ray diffraction techniques, J. Appl. Phys. 89 (1) (2001) 662–668.
[150] L.H. Cohen, G.C. Kennedy, Melting of copper, silver, and gold at high pressures, Phys. Rev. 145 (2) (1966) 519–525.
[151] N.R. Mitra, D.L. Decker, H.B. Vanfleet, Melting curves of copper, silver, gold, and platinum to 70 kbar, Phys. Rev. 161 (3) (1967) 613–617.
[152] D. Errandonea, The melting curve of ten metals up to 12 GPa and 1600 K, J. Appl. Phys. 108 (3) (2010) 033517–033610.
[153] S. Japel, B. Schwager, R. Boehler, M. Ross, Melting of Copper and nickel at high pressure: The role of d electrons, Phys. Rev. Lett. 95 (16) (2005) 167801.
[154] H. Brand, D.P. Dobson, L. Vočadlo, I.G. Wood, Melting curve of copper measured to 16 GPa using a multi-anvil press, HPR. 26 (3) (2006) 185–191.
[155] Q. An, S.N. Luo, L.B. Han, L. Zheng, O. Tschauner, Melting of Cu under hydrostatic and shock wave loading to high pressures, J. Phys: Condens Matter. 20 (2008) 095220.
[156] V.V. Huang, N.T. Hai, Investigation of the melting temperature of metal at various pressures. J. Phys. Soc. Jpn. 66 (1997) 3499; (Copyright (C) 1997 The Physical Society of Japan).
[157] A.B. Belonoshko, R. Ahuja, O. Eriksson, B. Johansson, Quasi ab initio molecular dynamic study of Cu melting, Phys. Rev. B 61 (6) (2000) 3838–3844.
[158] L. Vočadlo, D. Alfé, G.D. Price, M.J. Gillan, Ab initio melting curve of copper by the phase coexistence approach, J. Chem. Phys. 120 (2004) 2872.
[159] R. Ahuja, S. Rekhi, B. Johansson, Theoretical prediction of a phase transition in Gold, Phys. Rev. B 63 (21) (2001) 212101.
[160] P. Söderlind, Comment on theoretical prediction of phase transition in Gold, Phys. Rev. B 66 (17) (2002) 176201.
[161] D. Batani, A. Balducci, D. Beretta, A. Bernardinello, T. Löwer, M. Koenig, et al., Equation of state data for Gold in the pressure range $<$ 10TPa, Phys. Rev. B 61 (14) (2000) 9287–9294.
[162] W. Holzapfel, Equations of state for Cu, Ag, and Au and problems with shock wave reduced isotherms, HPR. 30 (3) (2010) 372–394.